

# Numerical Simulation of Eulerian Approach to Heat Transfer Performance of DCCLHPs through Leading-Edge Aircraft for Anti-Icing Applications

Mr. P. Mohanraj, *Research Scholar, Department of Mechanical Engineering, Vels Institute of Science, Technology & Advanced Studies(VISTAS), Chennai-600117, Taminadu, India*

Dr. R. Sridhar, *Assistant Professor, Department of Mechanical Engineering, Vels Institute of Science, Technology & Advanced Studies(VISTAS), Chennai-600117, Taminadu, India. (Email: srisampangy@gmail.com)*

## Article Info

Volume 82

Page Number: 7711- 7721

Publication Issue:

January-February 2020

## Abstract:

A numerical model were developed to heat transfer characteristics of a nanofluid on aircraft leading-edge anti-icing applications and predict the optimized flight operating parameters .This simulation presents a Eulerian approaches to flow the nanofluid with different volume fractions through DCCLHPs for leading aircraft anti-icing applications. The validation process offered the accuracy of the numerical results when compared with the experimental results. In Computational Fluid Dynamics (CFD) designed leading-edge structure and boundary meshing leads to diminish the grid sizes and improve the heat transfer performance and develop the wall treatment. The theoretical analysis of calculated surface temperature value is compared with the similar flight data experiments. As a result indicates the surface temperature on leading-edge skins discovered the interactions of hot/cold flow and thermal conductivity of solid to fluid zones. These computational results under the various flight conditions provide valuable suggestions for developing the anti-icing technologies.

## Article History

Article Received: 18 May 2019

Revised: 14 July 2019

Accepted: 22 December 2019

Publication: 04 February 2020

**Keywords:** *volume fraction, surface temperature, thermal conductivity, nanofluid, computational fluid dynamics*

## I. INTRODUCTION

The recent invention of flight safety is an important aspect in developing the aircraft anti-icing technologies. So far recent researches in aircraft industry aimed to focus and improve the inferior altitude local aircraft and decrease the anti-icing aircraft accidents [1]. On the other hand, remarkable effects of super cooled droplets have been addressed to the icing community and check the ecological issues and using simulation to fulfill the minimum requirements. Such that effect reanalysis the design and monitored the engineering problems and official recognition to undertaken the icing problems at in-flight conditions. Previous research investigates the causes of aircraft anti-icing by super cooled large

droplets. Bourgault et al (2000) reported numerical analysis of aircraft ice accretion by using FENSAP-ice based Computational Fluid Dynamics (CFD) software. They are using Eulerian approach as dual phase flow in a three dimensional representation of droplets on aircraft and engines. The dual phase flow consists of water droplets wished-for new Lagrangian particles based approach in anti-icing techniques. This investigation presents code validation for three dimensional models as results compared to the NASA experimental results and established the accuracy of the numerical model. The partial differential equations are often used to formulate the algorithm found for the 3D model by Navier stroke equation to anti-icing effects. Isaac et al (2001) also published the results by using

computational method to analyze the icing accumulation on aircraft wings by utilizing Eulerian approach

Generally leading-edges are easily affected by the ice accretion, due to the external flows causes over the surfaces temperature gradients and velocity and through disclosure to the upcoming flows. Most of the researcher's preferred to choose DCCLHPs thermal system on the aircraft leading edge anti-icing applications. Lin et al (2010) investigated the Dual Compensation Chamber Loop Heat Pipe (DCCLHPs) flow characteristics within the chamber and evaporator. They studied startup and steady state performance of loop heat pipe and manipulate vapour-liquid temperature distributions, surface temperature and performance of DCCLHPs.

Recent emerging trends are followed and need to develop the Computational Fluid Dynamics (CFD) results that can be possibly to achieve the superior design for aircraft anti-icing technologies [4]. The computational methods enhanced with the different theoretical formulations and solve the many engineering problems for the complex physical phenomenon of the object. The icing geometries of a complex flows are challenging techniques in the computations methods. Thus the system also analyzed the engine performance, flow through the wings, and nozzles etc.

For the ice preventions on aircraft wing ensure that the thermal anti-icing technologies both the experimentally and numerically. The thermal systems involved in the anti-icing operations under the different flight operating conditions are investigated by Brown et al (2003). Thus the three dimensional physical model enhance the better heat transfer performances by utilizing the air as a primary fluids. Current scenario of numerical analysis achieved the prominent airflow through the gas turbine engines. The airflow demonstration in a propulsion system made some reviews about anti-icing numerical methods, as a results suggested by the same reviews presented other researchers at the same time period [4, 6]. The anti-icing technology has found some incomplete ways in

designs such as highly developed CFD algorithms; interaction between the fluid-solid interfaces, CAD oriented views, multidisciplinary optimization, concurrent engineering approaches and the development of aerodynamic design process.

The simulation of in-flight conditions consisted several factors such as predicted ice accretion, heat load for icing and de-icing limits, codes for droplet impingement and routine dreadful conditions calculations. The predictions of droplet impingement method of calculations are agreed by Eulerian approach, incompressible potential flows and coupled boundary layer techniques [7-8]. Some of the researchers using Lagrangian approach for anti-icing simulation carried out and done on with the droplets tracking. Thus the size and shape of the ice accretion found by wind tunnels experimentally and predicted with inviscid flow using boundary layer techniques [9-10]. The icing codes of viscous-inviscid flow interactions addressed to the performance degradation calculation and heat transfer characteristics done on with the two dimensional model. The thermodynamic analysis of a two dimensional ice accretion model code formulated near to the surface streamlines [11-14]. Furthermore, three dimensional quasi models are proposed to develop the anti-icing technologies numerically. However, still needs to the capability for simulating droplet impingement an icing and deicing process, coupled interactions with the three dimensional model, viscous, compressible and incompressible flows are not readily exists. The continue representation of viscous-inviscid interactions were obtained the acceptable results on airfoils and not justified for the three dimensional model due to high capability of turbulence model presents.

The Lagrangian approaches of droplet tracking impingement proposed differential numerical techniques with the icing codes are able to required five grids [7]. These methods want to make a painstaking launching for every droplet upstream of an object and tracking the each droplet. On the other hand, Lagrangian method requires the velocity of the droplet path along the summation of individual

panel's hand-outs, each knots of arbitrary path and it is somewhat expansive. It could be found to increase the velocity spatial revival from the panels to use recalculation for determined the velocity vector by using the rectangular grids in three dimensional analyses importance to the Lagrangian droplet tracking method. The panel method also used to calculate the surface velocities over a flow due to the cost effectiveness. In addition the efficiency of the fitted geometry results collectively through implementation and addressed carefully in three dimensional model in order to avoiding insufficient inordinate particles are launched. So as the droplet impingements limitations also predicted along with the density and positions of the newly launched particles and capacity to calculate other thermodynamic factors on various components such as wings and flap during the climb state or descent. Still now the panel methods are improved the mesh accuracy for particle prediction and avoid the complex trajectory as it surface singularities and impact of droplet impingement.

So far, ice accretion of most readily presents a unidirectional control volume based approach that could not be accounted any geometrical features such as freezing, melting and beading process. However, limited approaches investigated the qualitative assessment of heat transfer analysis to the simple geometries and not established detailed futures about icing and anti-icing techniques. In this investigation designed and simulated a three dimensional model of NACA 0024 aircraft leading edge under the different AOA -50, 00 and +50 and various concentrations of nanofluids 25%, 50% , 75% and 100% for anti-icing applications. The traditional CFD tool was used to develop the heat transfer performance of nanofluid on aircraft leading-edge through DCCLHPs system. This simulation was presented more accurately and easily correlated with all thermodynamic factors. The structured grid type also presents to reduce the grid cell number for increase the simulation accuracy. From the numerical analysis and validation process ensures that the results conformity of heat transfer, thermal conductivity and surface temperature over a

leading edge skins and heat transfer characteristics under the different flight operating conditions. The DCCLHPs placed the inlet and exhaust configurations established based on the knowledge of thermal mechanism for anti-icing method developments. These investigations of major influencing factors are good agreed with the experimental results such as surface temperature, hot/cold flow mixtures, and heat transfer ability and thermal conductivity.

Table1. Geometrical characteristics of experimental LHP

Evaporator	values
Thickness (mm)	1.5
Length/width (mm)	40/30
Groove thickness (mm)	1
Fin number	18x15
Fin width (mm)	1x1
Wall	
Thickness (mm)	1.5
Porous sheet thickness(mm)	0.5
Compensation chamber	
Length/width (mm)	34.5/30
Height (mm)	6
Porous wick	
Length/width/thickness (mm)	36.5/30/4
Material	316L
Parameter of mesh	500, 82 layers
Vapor line	
Diameter (O/I)(mm)	6/4
Length (mm)	320

Liquid line	
Diameter (O/D)(mm)	6/4
Length (mm)	530
Condenser	
Diameter (O/D)(mm)	6/4
Length (mm)	810
Fin thickness (mm)	0.05
Fin length/width (mm)	100/20
Fan rotate speed (rpm)	3000

Table 2 Al<sub>2</sub>O<sub>3</sub>-water Nanofluids

Material Properties	Al <sub>2</sub> O <sub>3</sub>	water
Specific heat (JKg <sup>-1</sup> K <sup>-1</sup> )	765	4179
Density(Kgm <sup>-3</sup> )	3970	997.1
Thermal conductivity	40	0.605
Size	7nm	

## II. MATHEMATICAL MODEL

The DCCLHPs consists of evaporator, condenser and compensation chamber and vapour/liquid transport lines are shown in figure. Therefore no vapour grooves are formed in the evaporator outer surface, as a replacement for wick made up of copper thin layer deposited at inside the evaporator wall cases. Further the heat load applied on the road to the evaporator of a thin layer wick and the evaporation process occurred inside surface of the wick. When the heat is rejected and the fluid condenses during the generation of vapour flows into the vapour line thorough evaporator casing. After the liquid fluid condensed, then enter into the both side of the compensation chamber passing through liquid line. So far the liquid is supplied to the evaporator wick throughout the porous layer and established a flow loop of DCCLHPs. The distribution of working fluid around the leading-edge has created a form of capillarity pressure urbanized in the evaporator wick

and there is no external forces are desired. The heat transported from the evaporator to compensation chamber usually possessed thermal conductivity and again the evaporation processed at interface porous barrier between the evaporator and compensation chamber (CC1 and CC2). On the other hand the heat released from the evaporator to CC significantly decreased, thus the nature could improved the operational stability and reliability of DCCLHPs.

The full experimental setup of DCCLHP evaporator, condenser and liquid/vapour line discretized into smaller elements is shown in fig.

The two phase flow of a working fluid is on saturation temperature  $T_{sat}$  and mass flow rate expressed by

$$\frac{dml}{dz} = \frac{h_{in} p_{in} (T_{wall} - T_f)}{h_{1v}} \quad (1)$$

### A. Theoretical equation

The distribution of droplet flow field as mentioned as a real flow fluid in an Eulerian coordinates form can be expressed as follows. Based on the Eulerian assumptions should be neglected the Magnus force and phase changing capabilities. Eulerian approach describes the two-phase fluid of same quantities of droplets are presented for this simulation. The conservation of continuity and moment equation can be expressed as follows and further the equation of energy cannot be solved for this operation.  $\frac{\partial \rho}{\partial t} +$

$$\frac{\partial(\rho v_x)}{\partial x} + \frac{\partial(\rho v_y)}{\partial x} + \frac{\partial(\rho v_z)}{\partial x} = 0 \quad (2)$$

$$\frac{\partial \rho v_x}{\partial t} + \frac{\partial(\rho v_x v_x)}{\partial x} + \frac{\partial(\rho v_y v_x)}{\partial y} + \frac{\partial(\rho v_z v_x)}{\partial z} = F_{Dx} \quad (3)$$

$$\frac{\partial \rho v_y}{\partial t} + \frac{\partial(\rho v_x v_y)}{\partial x} + \frac{\partial(\rho v_y v_y)}{\partial y} + \frac{\partial(\rho v_z v_y)}{\partial z} = F_{Dy} + F_{GB} \quad (4)$$

$$\frac{\partial \rho v_z}{\partial t} + \frac{\partial(\rho v_x v_z)}{\partial x} + \frac{\partial(\rho v_y v_z)}{\partial y} + \frac{\partial(\rho v_z v_z)}{\partial z} = F_{Dz} \quad (5)$$

Where  $\rho$  – Droplet density

$$\rho = \alpha_v \rho_w \quad (6)$$

$\alpha_v$  – volume fraction,  $\rho_w$

– density of water,  $v_x, v_y, v_z$

– velocity of the droplet.

## B. Fluid flow

The fluid flow on the aircraft leading edge is described by Navier-stroke equation. This formulation of direct solution for the complex problem is very difficult to found out from the theoretical analysis. In order to avoid the complex term in this simulation using an alternative to apply Reynolds averaged method and k-ε turbulence model ((Fu and Farzaneh, 2010).

The heat transfer equation in the evaporator for the three dimension model can be expressed as follows

$$\frac{\partial^2 T_b}{\partial x^2} + \frac{\partial^2 T_b}{\partial y^2} + \frac{\partial^2 T_b}{\partial z^2} = 0 \quad (7)$$

The evaporator and double compensation chamber is investigated based on the velocity  $3 \times 10^{-4}$  and  $2 \times 10^{-2}$  m/s and based on the absorption noted by the changes under the heat load varied from 20w-1200w. This effect of small filtrations rate in temperature of the wick and as a secondary wick in the liquid line get equalized temperature. When the portraying thermal process describes the procedure can take advantage of the wick is shown in [17, 18], where for example stationary wick with the heat transfer condition expressed by the author.

$$\frac{\partial^2 T_w}{\partial x^2} + \frac{\partial^2 T_w}{\partial y^2} + \frac{\partial^2 T_w}{\partial z^2} = 0 \quad (8)$$

During the liquid filtration in the course of wick enhanced with the energy balance by the convective component of heat transfer for the boundary conditions stated below

Heat applied to the evaporator surface ( $\Omega_q$ ):

$$-k_b \frac{\partial T_b}{\partial y} = q_{load} \quad (9)$$

Heat flux also distributed uniformly

$$q_{load} = \frac{Q_{load}}{L_q \times B_q} \quad (10)$$

Heating area  $L_q \times B_q$  – (length)  $\times$  (breadth)

Similarly at the evaporator surface of the wick consists of performed as a vapour groove and end the wick connected to the compensation chamber.

The dried condition has full filled for the use made of

$$K_w \cdot \frac{\partial T}{\partial n} \Big|_{\zeta} = 0 \quad (11)$$

Described the boundary between the wet area and dry area

$$K_{eff} \cdot \frac{\partial T_{wick}}{\partial n} \Big|_{wet} = K_w \cdot \frac{\partial T_{wick}}{\partial n} \Big|_{dry} \quad (12)$$

Outer surface on the evaporator  $\Omega_{amb}$

$$-K_b \cdot \frac{\partial T}{\partial n} \Big|_{\zeta} = \alpha_{amb} \cdot (T_{\zeta} - T_{amb}) \quad (13)$$

Similarly for inner surface of the compensation chamber

$$-K_b \cdot \frac{\partial T}{\partial n} \Big|_{\zeta} = \alpha_{in\_cc} \cdot (T_{\zeta} - T_{cc1}) \quad (14)$$

$$-K_{eff} \cdot \frac{\partial T}{\partial n} \Big|_{\zeta} = \alpha_{in\_cc} \cdot (T_{\zeta} - T_{cc1}) \quad (15)$$

The energy equation for the evaporator can be expressed as follows.

$$Q_{load} = Q_{cc1} + Q_{cc2} + Q_{amb} + Q_{cp} + Q_{ev} \quad (16)$$

Internal heat exchange coefficient

$$Q_{cc1} = \int_{\Omega_b}^0 q_{\zeta} d\Omega + \int_{\Omega_d}^0 q_{\zeta} d\Omega \quad (17)$$

Total heat flow processed to the evaporator  $Q_{amb} = \int_{\Omega_{amb}}^0 q_{\zeta} d\Omega \quad (18)$

$Q_{cp}$  Is mentioned convective heat transfer in the wick, it can be processed the liquid transport from CC to evaporator at the wall surface. This can be described turbulence in the evaporator

$$Q_{cp} = C_p \int_{\Omega_{ev}}^0 m_{\zeta} (T_{\zeta} - T_{cc}) d\Omega \quad (19)$$

Where  $T_{\zeta}$  –liquid temperature

$$m_{\zeta} = \frac{q_{\zeta}}{h_{hv}} \quad (20)$$

Total vapour heat generation

$$Q_{ev} = \int_{\Omega_{coll}}^0 q_{ev} d\Omega + \int_{\Omega_{vg}}^0 q_{ev} d\Omega \quad (21)$$

## C. Grid generation

The complicated structure of DCCLHPs has been discretized by unstructured grid in the ICFM CFD commercial software. It is most widely used in the solving complex problem with complex flow around the problems. This anti-icing CFD simulation analyzed the three dimensional of a inlet/outlet flows,

heat transfer characteristics of a nanofluids, viscosity, thermal conductivity during the heat transfer near to the wall surfaces, less solver time with expected accuracy of the computational methods and grid generations are monitored. The generations of unstructured grid using ICEM mesh successfully converted into structured grid for make an internal/external flow fluid through anti-icing applications. The representation of structured grid on aircraft leading-edge is shown in Fig 1. Thus the mesh refinement has near to the impingement sections and the interior grid also bounded by a boundary layer meshed regions. The internal and external solid surfaces of meshes are connected with suitable aspect ratio, where the mesh is exists. The aluminium interior skins are utilized by the structural mesh for calculating thermal conductivity. The entire system consists of 521664 hexagonal cells, but it is always less than the unstructured grid for similar resolution.

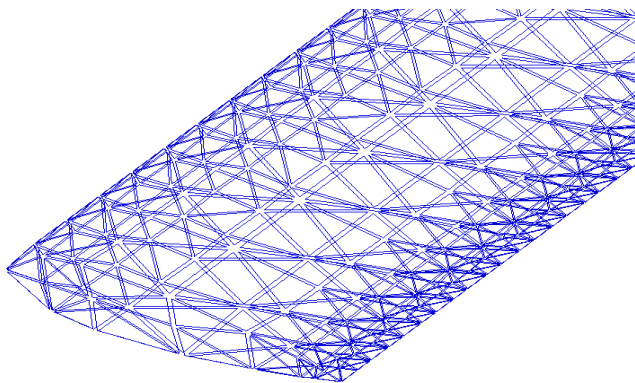


Fig.1 Grid generation

#### D. Time step analysis

As ice amasses at higher altitude, its form changes, altering the airway until the water gathering esteem recently processed is never again substantial. In case of past thermodynamic data's could be found ice growth rate and it has stopped to analyze the new flow simulations. This shortest time of increments leads to convert into large computational time. Interestingly, the mistake for quite a while step can be huge to such an extent that the anticipated ice shape can fluctuate altogether from the real environmental conditions. In order to avoid this problem using LEWICE code based on the previous

numerical analysis from the literature surveys [19]. It can be designed based on the original data's that communication to the dimensionless ice thickness. This value predicted from the coefficient of water collections and flow field parameters in the extreme filed. The time-step equation expressed by follows

$$\Delta t = \frac{A_c \rho_i}{\beta_{\max} V_{\infty} LWC \left(1 + \frac{\phi}{20}\right)}$$

Where  $\rho_i$  -ice density,  $A_c$  - Accumulation parameter (0.01) utilized in the LEWICE code.

### III. RESULT AND DISCUSSION

The primary part of CFD three dimensional Eulerian models describes the capability of design development for anti-icing system. Present investigation carried out the simulation on NACA 0024 airfoil leading-edge and wind tunnel model GLC-305 under different flight conditions, analyze the surface temperature and heat transfer characteristics, working assessment of DCCLHP and design modifications. As for the simulation results discussed in details established in below the sections.

#### A. Surface Temperature

Primarily the surface temperature distributions effects have been analyzed due to change of flow speed and Angle of Attack (AOA) as for the corresponding boundary conditions. From the graphical representation is shows in Fig 2 of surface temperature on leading-edge upper surface over the skins under the flight conditions  $\alpha$  (-50, 00, 50 and 100) and flight speed (-13.4, 21.2 and 34.6 m/s as per the experimental conditions) respectively. When increasing Angle Of Attack (AOA) causes the surface temperature obtained lower value on surfaces and higher value on upper surfaces. The heavier drop of the top face temperature is because of the relating increment of the outside speed over the upper surface. Similarly obtained coefficient of surface heat transfer on the lower surfaces, however compared with upper surface increased significantly near at the curved shape of the leading edge where the velocity reached to maximum limit. As results established when the AOA changes to must involve in the

characterizing of surface heat transfer coefficient (SHTC). Wherever increasing Mach number could decrease the external temperature at near the leading-edge and closely related to the end of the bay for the reason generation of additional heat supplied to the external fluids. It is fascinating to see that the SHTC esteems for the upper surface increment just about a comparative the sum, mirroring the general stream speeding up because of the expansion of Mach number. The temperature difference has been maintained flexibly that the heat flux from the Loop heat pipe (LHP) were increased both the inlet temperature and pressure together increasing separately. Thus the surface temperature plots could be seen that has increased both T0 and P0, it has obtained little over heating on lower side and under heating on upper surface of the leading –edge. So far suggesting changes made either T0 or P0 for same amount of heat flux increases would leads to changes of the surface temperature. In Fig 3 shows the graphical representation of outside surface temperature in the leading-edge skin under the AOA +50.

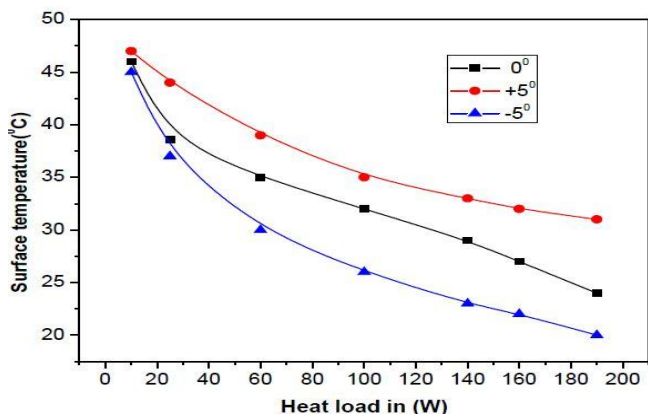


Fig.2 Leading edge Surface temperatures

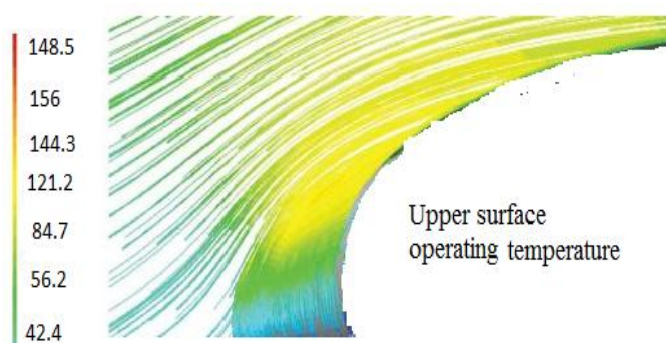


Fig.3 Flow through leading-edge for anti-icing  
Correlations are given of the inlet mass flow rate

and total heat transfer through all the liquid line and vapour lines on DCCLHPs anti-icing system. Even thought increasing AOA for the further cases increased the exhaust pressure at lower surface of the exits flow location and inlet heat flux flow slightly reduced during the flow separation to all liquid lines. In the interim, more heat was brought away by the outside streams as the upper surface velocity expanded. When increasing T0 and P0 in a maximum limit would causes to increases both mass heart transfer and mass flow rates from the LHP. The thermal efficiency, determined by the normal static temperature esteems at the LHP liquid lines and as the far-field static temperature, gives a comparable examination result. The thermal efficiency increments when more warmth is moved to the outer moves through the skin, yet not really mirror the skin temperature levels.

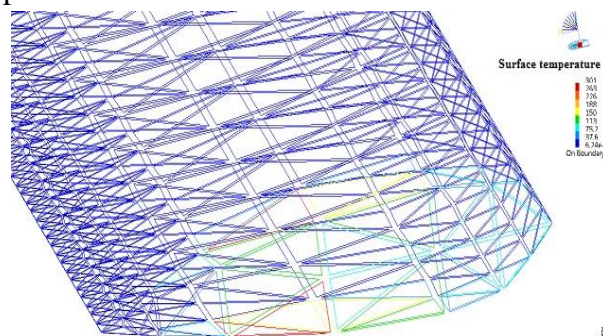


Fig. 4 Thermal characteristics of working fluid (AOA +50)

The properties of nanofluids Al2O3, thermal conductivity, temperature, velocity, pressure, latent heat evaporation, viscosity and surface tension referred from the previous experimental works. This phenomenon used to calculate the temperature difference of the working fluid range from 10 to 2000 C. Cubic spline interpolation function was used to interpolate the temperature difference  $\Psi=f(T)$ . The nodal temperature of all grid structure might be controlled each time step of the analysis were made by the thermophysical properties of the nanofluids shows in Fig 5. As a result calculated the functional dependence of nodal temperature perceived by number of iterations follows in the time steps. Where  $\Psi$ - thermophysical parameter expressed as follows.

$$\Psi_{i,j,k}^N = f(T_{i,j,k}^{N-1})$$

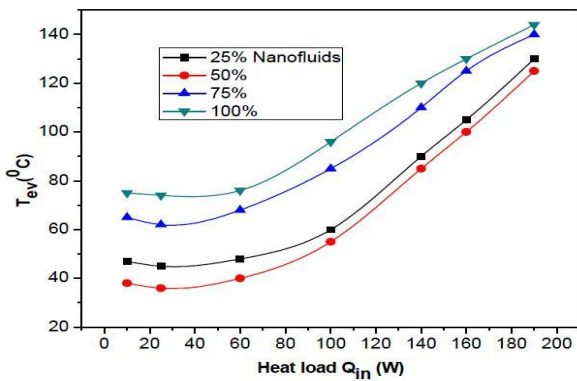


Fig. 5 Temperature at evaporator with different % of nanofluid concentrations

The +15 deg infusion cases reduce the bottom surface temperature, while the -15 deg model diminishes the top surface temperature. Hence, the aftereffects of these two cases propose that 1) changing the infusion headings could change the skin surface temperature profile and 2) the decrease of the absolute powerful impingement zone of the sight-seeing on the inward surface will lessen the complete warmth move from the sight-seeing to the skin and result in a temperature decline over the exterior surfaces. The subsequent endeavor is to bring the fumes openings from the lower skin to the back shield close to the upper-back corner of the narrows to carry more warmth to the upper side.

### B. Wick thermal conductivity

In Fig 6 shows the effect of thermal conductivity on wick for the corresponding heat load from evaporator to the compensation chamber. The fixation of heat flux in the wick is more important for the LHP process and it has been neglect the heat transfer to the evaporator and heat losses. From the numerical results concluded the effect of decreasing thermal conductivity leads to increase the higher temperature in the system. When utilizing high load, the wick material is always well-defined for the same operating conduction. Therefore, the process of wick characterized by two ways such as diminishing the wick conductivity lessens the piece of heat through the permeable structure, along these lines prompting a lower transversal heat flux. At the point when the vanishing warmth move at the contact line between the blade, the section and the wick is

constrained or when a high warm contact the obstruction exists between the balance and the permeable material, heat must be directed through a more drawn out way in the wick so as to be dissipated.

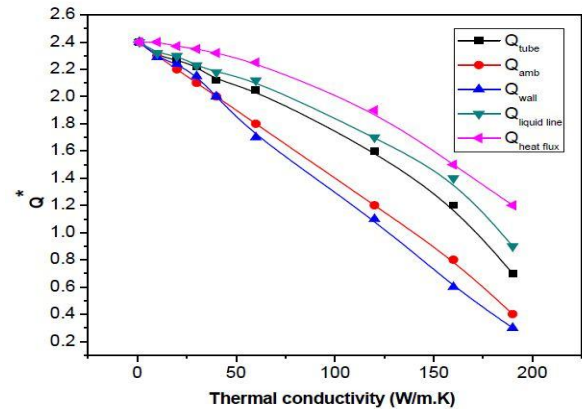


Fig.6 Wick thermal conductivity on DCCLHP anti-icing

### C. Vapour and Liquid line thermal conduction

In Fig 7 shows the thermal conductivity and effect of neglecting heat losses from the evaporator to the ambient temperature. The high conductivity of the material was used to improve the performance of LHP and also the larger sections in LHP need to be cooled by the reason of heat dissipation. At high info controls the thing that matters isn't critical and the thermal conduction through the fluid transfer lines doesn't emphatically impact the LHP activity. Further the lower input power is consumes low mass flow rate when the fluid flow transferred from evaporator to the condenser. Generally the vapour grooves have super heat limited at the end of the evaporator and vapour flow line cooled as heat losses convert into ambient conditions.

Consequently, the existing vapors are already condensed in the vapour line before passing through the condenser. At that point, the liquid temperature is equivalent to the immersion temperature and the high inward hating coefficient will in general force the temperature of the vapor to the divider until the passageway of the condenser.

On account of a copper fluid line, a huge length of the cylinder divider is heat by conduction from the reservoir. The fluid coming back to the remuneration

chamber is then at a higher temperature  $T_{res}$ , in, giving a low heating effect. Since the fluid coming back to the condenser is subcooled, a lot of heat is led from the evaporator in the course of fluid line to be dispersed in contact with the fluid streaming in the cylinder. Heat conduction in the loop line divider is practically immaterial and the fluid line is colder compared with a copper line. Subsequently, the heat misfortunes to the encompassing abatement and changing flexibility to the LHP working temperature are high when the fluids are in high velocity.

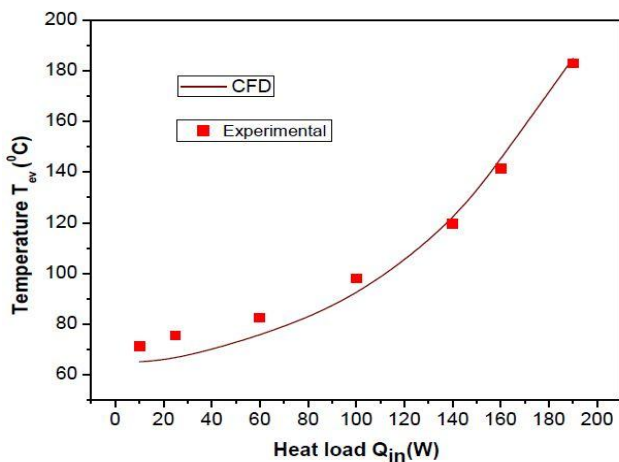


Fig.7 Evaporator temperature comparisons with experimental numerical data's

However, higher heat load in condenser possessed low temperature on to the condenser because of the heat transfer difference between the fluid and liquid lines as shows in Fig 8. Toward the start of the condenser, the condensation process will leads a force the temperature to the evaporator wall. The liquid is heating before passes through reservoir because of thermal conduction from the reservoir. In this way, the divider and the fluid temperatures are nearer to the supply temperature than at low heat loads and the vehicle line material has a minor impact, the fluid heat being practically consistent at all the conduction in the cylinders.

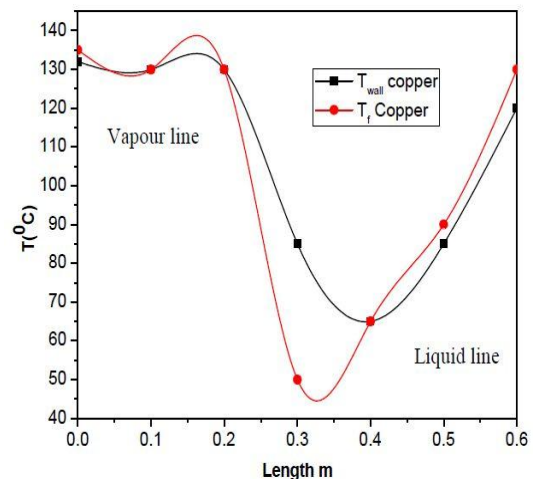


Fig.7 Temperature distributions along the Transport lines for heat load 100W

### 3.4 Heat transfer in the evaporator

In Fig 9 shows the heat flux in the evaporator by applying the het load  $Q_{in}$  from 30W to 1000w without the effect of heat losses. The copper material is used to design of the evaporator casing and the wick tends to nickel material due to the effective thermal conductivity which is almost equivalent to the 5.4 ( $W\ m^{-1}K^{-1}$ ). From the analysis experiences more than 85% of heat dissipation occurred in the evaporator and remaining heat is converted into vapour/liquid lines. Even though, the parasitic heat flux in the course of the wick always equal to the applied heat load. Similar heat transfer rates are under 1%, affirming that more heat is directed through the fluid line than through the vapor line. It shows up likewise that when the increasing heat loads, the vanishing rate is upgraded and heat misfortunes through the fluid line are less huge.

Besides the evaporator temperature is different due to the heat load variations in wall to ambient conditions. As results obtained heat transfer in the evaporator range from 60-80%. So far the reservoir temperature is high and also the evaporator both of value induced 20% of total heat flux value. Heat misfortunes to the surrounding are less predominant for large amount of heat loads though the all-out of heat flux and the dissipation rate are improved.

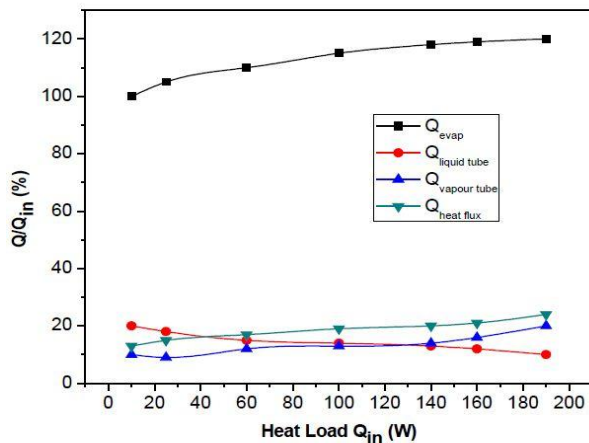


Fig.7 Heat transfer in the DCCLHP system

#### IV. CONCLUSION

The present investigation summarize the major influencing effect of nanofluid concentrations under the different operating parameters utilizing three dimensional DCCLHPs thermal anti-icing system through leading edge airfoil NACA 0024. In this case of investigate the internal/ external flow fluids with the benefits of thermal conductivity through the solid surfaces by using FLUENT in Computational Fluid Dynamics (CFD). This CFD analysis exhibit the some features for development to the anti-icing system, thus the features include structured/unstructured grid, super cooled droplets impingements and conductive heat transfer simulations. The major advantage of using Eulerian formulation in CFD is leads to improve the efficiency of the thermal analysis for the corresponding boundary conditions. There is a no method used for tracking particle locations due to avoiding uncertainty problem in three dimensional fluid flow simulations. Furthermore, the effect of applied heat load causes a concentrated heat supply through the evaporator operating temperature of an Al<sub>2</sub>O<sub>3</sub>-water working nanofluid loop heat pipe and heat transfer on the wick was performed.

The temperature of the evaporator was calculated to the corresponding applied heat load as a range from 20W to 250 W respectively. Similar examinations of trial information and reproduction results have demonstrated that the model satisfactorily depicts thermal procedures in the

evaporator furthermore, might be utilized for dissecting the presentation qualities of LHPs. Reproductions demonstrate the significant impact of the heat transfer coefficient and of the wick conductivity on the LHP working temperature just as on the temperature field possessed in the evaporator. Furthermore, a low vanishing coefficient prompts a huge increment on top of it working temperature.

#### V. REFERENCES

- [1] "FAA In-flight Aircraft Icing Plan," Federal Aviation Administration, U.S. Dept. of Transportation, Washington, DC, April 1997.
- [2] Isaac, G. A., Cober, S. G., Strapp, J.W., Korolev, A.V., Tremblay, A., and Marcotte, D. L., "Recent Canadian Research on Aircraft In-Flight Icing," Canadian Aeronautics and Space Journal, Vol. 47, No. 3, 2001, pp. 213–221.
- [3] Bourgault, Y., Boutanios, Z., and Habashi, W. G., "Three-Dimensional Eulerian Approach to Droplet Impingement Simulation Using FENSAPICE, Part 1: Model, Algorithm, and Validation," Journal of Aircraft, Vol. 37, No. 1, 2000, pp. 95–103.
- [4] Effect of Icing, De-Icing, and Heavy Rain on Aircraft Performance," AGARD Fluid Dynamics Panel, FDP Working Group 20, Advisory Group for Aerospace Research and Development, NATO, 1997.
- [5] Brown, J. M., Raghunathan, S., and Watterson, J. K., "Heat Transfer Correlation for Anti-Icing System," Journal of Aircraft, Vol. 40, No. 1, 2003, pp. 65–70.
- [6] Sindir, M., and Lynch, E., "Overview of the State-of-the-Practice of Computational Fluid Dynamics in Advanced Propulsion System Design," AIAA Paper 97-2124, June 1997.
- [7] Hedde, T., "Modélisation tridimensionnelle des dépôts de givre sur les voilures d'aéronefs," Ph.D. Thesis, Dept. des Sciences de l'Atmosphère, Univ. Blaise Pascal, 1992.
- [8] Ruff, G., and Berkowitz, B., "Users' Manual for the NASA Lewis Ice Accretion Prediction Code (LEWICE)," NASA TR 185129, 1990.
- [9] Potapczuk, M., Al-Khalil, K., and Velazquez,

- M., "Ice Accretion and Performance Degradation Calculations with LEWICE/NS," AIAA Paper 193-0173, Jan. 1993.
- [10] Wright, W., and Potapczuk, M., "Comparison of LEWICE 1.6 and LEWICE/NS with IRT Experimental Data from Modern Airfoil Tests," AIAA Paper 97-0175, Jan. 1997.
- [11] Sankar, L., Phaengsook, N., and Bangalore, A., "Effects of Icing on the Aerodynamic Performance of High Lift Airfoils," AIAA Paper 93-0026, Jan. 1993.
- [12] Airfoils," AIAA Paper 97-2235, June 1997. 10Kwon, O., and Sankar, L., "Numerical Investigation of Performance Degradation of Wings and Rotors due to Icing," AIAA Paper 92-0412, Jan. 1992.
- [13] Dompierre, J., Cronin, D. J., Bourgault, Y., Baruzzi, G., and Habashi, W., "Numerical Simulation of Performance Degradation of Ice Contaminated.
- [14] Lee, S., Dunn, T., Gurbacki, H., Bragg, M., and Loth, E., "An Experimental and Computational Investigation of Spanwise-Step-Ice Shapes on Airfoil Aerodynamics," AIAA Paper 98-0490, Jan. 1998.
- [15] G.P. Lin, N. Li, L.Z. Bai, et al., Experimental investigation of a dual compensation chamber loop heat pipe, International Journal of Heat and Mass Transfer 53 (15-16) (2010) 3231-3240.
- [16] Fu, P., Farzaneh, M., 2010. A CFD approach for modelling the rime-ice accretion process on a horizontal-axis wind turbine. J. Wind Eng. Ind. Aerodyn 98, 181–188.
- [17] E.I. Altman, M.Ia. Mukminova, H.F. Smirnov, The Loop Heat Pipe Evaporators Theoretical analysis, Proceedings of the 12th Int. Heat Pipe Conference, Moscow, Russia, 2002, pp. 159e164.
- [18] C. Figus, Y. Le Bbray, S. Bories, M. Prat, Heat and mass transfer with phase change in a porous structure partially heated: continuum model and pore network simulations, international Journal of Heat and Mass Transfer 42 (1999) 2557e2569.
- [19] Wright WB. User's manual for the improved NASA LEWIS ice accretion code LEWICE

1.6. 995. NASA CR 198355